PCCP

PAPER

View Article Online
View Journal | View Issue

Cite this: *Phys. Chem. Chem. Phys.*, 2015, **17**, 17778

On the role of local charge carrier mobility in the charge separation mechanism of organic photovoltaics†

Saya Yoshikawa,[a] Akinori Saeki,*[ab] Masahiko Saito,[c] Itaru Osaka[bc] and Shu Seki*[ad]

Received 19th March 2015,
Accepted 27th May 2015

DOI: 10.1039/c5cp01604e

www.rsc.org/pccp

Although the charge separation (CS) and transport processes that compete with geminate and non-geminate recombination are commonly regarded as the governing factors of organic photovoltaic (OPV) efficiency, the details of the CS mechanism remain largely unexplored. Here we provide a systematic investigation on the role of local charge carrier mobility in bulk heterojunction films of ten different low-bandgap polymers and polythiophene analogues blended with methanofullerene (PCBM). By correlating with the OPV performances, we demonstrated that the local mobility of the blend measured by time-resolved microwave conductivity is more important for the OPV output than those of the pure polymers. Furthermore, the results revealed two separate trends for crystalline and semi-crystalline polymers. This work offers guidance in the design of high-performance organic solar cells.

Introduction

Due to the compelling prospect of renewable energy sources, there is currently a growing interest in the development of organic photovoltaic (OPV) cells.[1,2] A bulk heterojunction (BHJ) framework is relevant to cost-effective roll-to-roll production[3] and comprises an intimate mixture of electron-donating conjugated molecules or polymers and electron-accepting fullerenes. For the last decade, significant progress has been made in the development of novel low-bandgap polymers[4] and device engineering,[5,6] which has evolved OPVs as a scientific and commercial enterprise. The power conversion efficiency (PCE) of OPV cells is susceptible to a complex ensemble of photoabsorption, exciton diffusion, charge separation (CS), and charge transport, which are all significantly affected by hierarchical morphology encompassing a variety of factors, such as orientation,[7] domain size,[8] miscibility,[9] and interfacial phenomena.[10] Therefore, the elucidation of the carrier generation and energy loss mechanisms underneath the BHJ architecture is of utmost importance in order to offer guidance in the design of high-performance OPVs.

The CS process competes with geminate recombination and plays a central role in photocurrent generation.[11,12] If the charge transfer (CT) exciton at the donor/acceptor interface[13,14] is formed after ultrafast electron transfer, then it must overcome the intrinsically strong Coulomb binding potential due to the low dielectric constant of organic materials. According to the Onsager–Braun model,[15] the efficiency of splitting into a CS state is considerably small ($<1\%$), even in the presence of a high external electric field. Nonetheless, experimental CS efficiency (η_{CS}) in most efficient OPVs exceeds 70% under short circuit conditions and sometimes reaches 100%. For instance, a blend of PCDTBT and phenyl-C_{71}-butyric acid methyl ester ($PC_{71}BM$) exhibits an internal quantum efficiency (IQE) that is almost unity.[16]

Recently, inquiry into this high η_{CS} has triggered numerous investigations. Using an ultra-short pump-and-push pulse technique, a hot CT exciton was found to leap over the uphill energetic landscape by the delocalisation of CT.[17] Such a large CT radius allows facilitation of its dissociation on the Onsager–Braun framework.[18] The entropy of an isotropic three-dimensional network and the role of the fullerene phase have a significant impact on the CS process,[19] as dictated from mostly less efficient non-fullerene acceptors in BHJ frameworks. The energy gradient from the mixed donor/acceptor phase to their respective pure domains[20] and relaxation in the density of states[21] are responsible for prompt and efficient CS. However, there is no consensus regarding the precise mechanism, but it is instead often material-specific and thus the subject of ongoing debate.

[a] *Department of Applied Chemistry, Graduate School of Engineering, Osaka University, 2-1 Yamadaoka, Suita, Osaka 565-0871, Japan. E-mail: saeki@chem.eng.osaka-u.ac.jp, seki@chem.eng.osaka-u.ac.jp*
[b] *Japan Science and Technology Agency (JST)-PRESTO, 4-1-8 Honcho Kawaguchi, Saitama 332-0012, Japan*
[c] *Emergent Molecular Function Research Group, RIKEN Center for Emergent Matter Science (CEMS), Wako, Saitama 351-0198, Japan*
[d] *Department of Molecular Engineering, Graduate School of Engineering, Kyoto University, A4-009 Kyoto University, Katsura Campus, Nishikyo-ku, Kyoto 615-8510, Japan. E-mail: seki@moleng.kyoto-u.ac.jp*

† Electronic supplementary information (ESI) available: Tables S1–S4 and Fig. S1–S9. See DOI: 10.1039/c5cp01604e

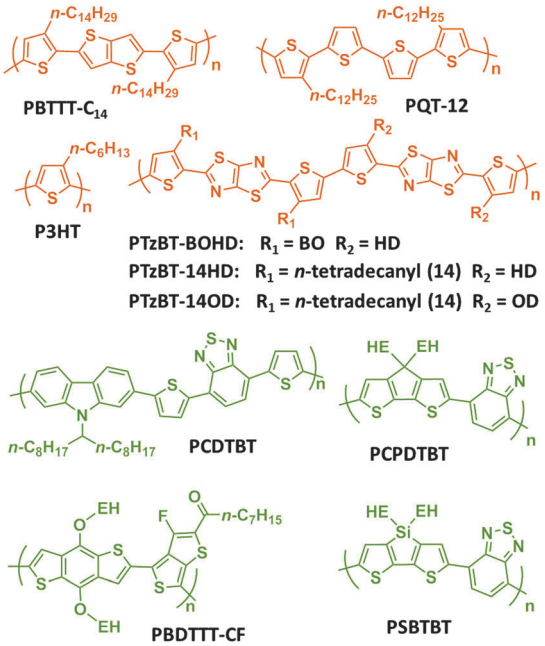

Fig. 1 Chemical structures of investigated OPV polymers. The branched alkyl chains are denoted as BO: 2-butyloctyl, HD: 2-hexyldecyl, OD: 2-octyldodecyl, and EH: 2-ethylhexyl. Crystalline and semi-crystalline polymers are coloured orange and green, respectively (see text regarding these categories).

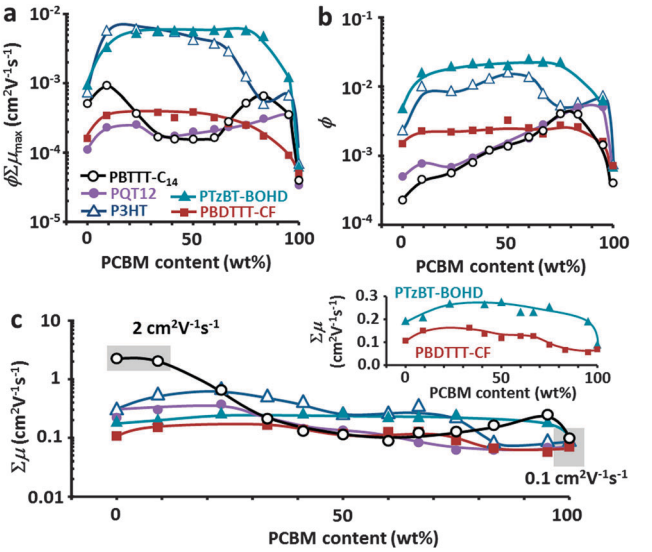

Fig. 2 Experimental determination of $\sum\mu$ in polymer:PCBM blend films by TRMC under 355 nm excitation (photon density = 4.6 × 10^{15} photons cm^{-2} $pulse^{-1}$). (a) Dependence of $\phi\sum\mu_{max}$ on the PCBM content. The PCBM contents of 0 and 100 wt% represent pure polymer and pure PCBM, respectively. (b) Dependence of ϕ on PCBM content measured using the PC technique. (c) $\sum\mu$ obtained by dividing $\phi\sum\mu_{max}$ by ϕ. The inset shows linear-linear plots of $\sum\mu$ for PTzBT-BOHD and PBDTTT-CF.

In this work, we have focused on the influence of the local charge carrier mobilities on the polymer–methanofullerene OPV. OPV cells with ten different conjugated polymers (Fig. 1) were evaluated using measurements by laser-flash time-resolved microwave conductivity (TRMC),[22,23] which employs a nanosecond laser for excitation and microwaves (*ca.* 9.1 GHz) as the alternating-current (AC) probe. One of the noteworthy aspects of laser-flash TRMC is a good correlation with the device performance of BHJ manifolds, even though it is a contactless evaluation.[24,25] In addition, the use of Xe-flash TRMC with a long (10 μs) pseudo-sunlight pulse results in improved correlation between the photoconductivity maxima ($\Delta\sigma_{max}$) and PCE divided by the open circuit voltage (V_{oc}) with four low-bandgap polymers,[26] PCDTBT, PCPDTBT, PBDTTT-CF, and PBDTTPD. The improved correlation enabled elucidation of the primary factor governing the overall device performance. Janssen *et al.* have pointed out that the presence of nanocrystalline domains with a high local carrier mobility of at least one of holes and electrons may explain the efficient dissociation of CT states.[27] Deibel *et al.* have also suggested that fast local charge carrier transport can explain the high experimental quantum yields in their kinetic Monte Carlo (MC) simulation and Onsager–Braun analysis.[28] To provide a link in the continuing chain of this issue, we investigate the effect of local mobility of crystalline or semi-crystalline polymers in BHJ films.

Results and discussion

Local mobilities dependent on p/n blend ratio

Fig. 2a shows the maximum $\phi\sum\mu$ (=$\phi\sum\mu_{max}$) of polymer:phenyl-C_{61}-butyric acid methyl ester (PCBM) blend films with various compositions, where $\sum\mu$ and ϕ are the sum of the positive and negative charge carrier mobilities (= $\mu_+ + \mu_-$), and the charge carrier generation efficiency at the pulse-end, respectively (kinetics are provided in Fig. S1, ESI†). For instance, in PBTTT-C_{14}, the two peaks are clearly resolved at 9 and 83 wt% PCBM, whereas the latter corresponds to the optimal device blend.[29] The first peak was significantly suppressed when the excitation wavelength was switched from 355 to 500 nm (Fig. S2, ESI†), which is consistent with the previous TRMC study of an identical polymer:$PC_{71}BM$ film excited at 550 nm.[29] The appearance of the first peak at 355 nm excitation is attributed to the wavelength dependence of ϕ rather than $\sum\mu$, which is likely pronounced when the energy difference between the highest occupied molecular orbital (HOMO) of the polymer (donor) and that of $PC_{71}BM$ or PCBM (acceptor) is small.[30] The use of PCBM with a stronger absorption than $PC_{71}BM$ in the UV region is one reason for the different wavelength dependence of ϕ.

In contrast, the ϕ dependence determined by the photocurrent (PC) technique[31] was converged to a simple convex feature that accompanied the single peak at 75–83 wt% PCBM (PBTTT-C_{14} : PCBM = 1 : 4–1 : 5), which is consistent with the optimal blend ratio in the OPV[32] (Fig. 2b). The PC transients for each blend are given in Fig. S3 (ESI†), all of which indicate excellent linearity with the applied bias and corroborate that the PC is not affected by the contact resistance or the space charge. Note that the obtained small ϕ values at 355 nm (10^{-4}–10^{-2}) compared to IQE of an OPV device under 1 sun result from the involvement of non-geminate recombination, due to the nanosecond time resolution and the orders of magnitude higher intensity of the laser pulse than sunlight.[26]

Dividing $\phi\sum\mu_{max}$ by ϕ affords $\sum\mu$ at the respective PBTTT-C_{14}:PCBM blend ratio (Fig. 2c). It is notable that $\sum\mu$ for the pure polymer is as large as 2 $cm^2\ V^{-1}\ s^{-1}$, which is of the same order as that assessed for hole mobilities in field-effect transistors (FET; 0.6–1 $cm^2\ V^{-1}\ s^{-1}$).[32,33] Notably, $\sum\mu$ immediately underwent a progressive decrease of one order of magnitude upon further addition of PCBM. Thus, it is reasonable to conclude that the decrease in $\sum\mu$ is due to PCBM intercalation,[34] as illustrated in Fig. S4 (ESI†), which inhibits polymer crystallization and elevates the energetic disorder of the conjugated system along the polymer chains. $\sum\mu$ for the pure PCBM film (PCBM = 100 wt%) was determined to be *ca.* 0.1 $cm^2\ V^{-1}\ s^{-1}$, which is reasonably consistent with 0.04–0.3 $cm^2\ V^{-1}\ s^{-1}$ for PCBM evaluated using pulse-radiolysis TRMC.[35] The constant $\sum\mu$ of *ca.* 0.1 $cm^2\ V^{-1}\ s^{-1}$ over the wide range of PCBM compositions indicates the predominance of electron mobility in PCBM clusters rather than hole mobility in the PBTTT-C_{14} phase in the observed TRMC transients, as discussed by Kopidaki *et al.*[29] More spatially separated charge carriers are generated above the threshold of the PCBM percolation network, which results in enhanced photocurrent in the OPV devices.

$\sum\mu$ for the other polymers was evaluated in the same manner. In the PQT-12:PCBM blends, the $\phi\sum\mu_{max}$ peak is located at the high PCBM composition (Fig. 2a), which is also explained by the intercalation of PCBM and the growth of PCBM clusters with an excess of PCBM.[36,37] This is supported by the requirement of high PCBM loading (*ca.* 80 wt%) to maximize the device performance with both PQT-12 and PBTTT-C_{14}. In sharp contrast, P3HT, PTzBT-BOHD, and PBDTTT-CF show a relatively flat dependence of $\phi\sum\mu_{max}$ on the PCBM content. Therefore, $\sum\mu$ for these polymers was evaluated on the basis of PC measurements (PC transients are given in Fig. S5, ESI†).

Fig. 2c shows the different impact of the PCBM concentration on $\sum\mu$ among the polymers. At low PCBM content, the crystalline P3HT and PQT-12 polymers exhibit high $\sum\mu$ values of 0.3–0.7 and 0.2–0.4 $cm^2\ V^{-1}\ s^{-1}$, respectively. These values correspond to their highest FET hole mobilities (0.1–0.2 $cm^2\ V^{-1}\ s^{-1}$)[38,39] and the highest mobility in P3HT determined by a combination of TRMC and transient absorption measurements.[31] However, $\sum\mu$ gradually decreases with the PCBM content in all polymers and approaches *ca.* 0.1 $cm^2\ V^{-1}\ s^{-1}$ for the pure PCBM film. Of particular interest is that the value of $\sum\mu$ for P3HT:PCBM at the optimal device ratio ([PCBM] = 50 wt%) is 0.26 $cm^2\ V^{-1}\ s^{-1}$, which is almost identical to the saturated $\phi\sum\mu_{max}$ of 0.22 $cm^2\ V^{-1}\ s^{-1}$ under exposure to a low excitation photon density ($<10^{13}$ photons cm^{-2}).[24] Therefore, this $\sum\mu$ is assumed to be composed of contributions from both holes in the polymer (*ca.* 0.1 $cm^2\ V^{-1}\ s^{-1}$) and electrons in the PCBM phase (*ca.* 0.1 $cm^2\ V^{-1}\ s^{-1}$). In contrast, $\sum\mu$ for PQT-12 was constrained to around 0.06–0.1 $cm^2\ V^{-1}\ s^{-1}$ for [PCBM] $>$ 50 wt%, which is a similar trend to that for PBDTTT-C_{14}:PCBM. In these intercalating-type polymers, electron mobility in PCBM clusters would significantly contribute to the value of $\sum\mu$. In contrast, P3HT polymers can self-assemble into lamellar domains during film formation and annealing, which pushes PCBM away from the crystalline P3HT domains.[40] This leads to the formation of pure P3HT and PCBM nanodomains concomitant with the formation of the semi-crystalline mixed phase. These hierarchical structures are relevant for efficient device operation[41] and the observed high local hole mobility is assumed to reflect the presence of such pure P3HT domains.

$\sum\mu$ for crystalline PTzBT-BOHD and semi-crystalline PBDTTT-CF indicated a weak dependence on the PCBM content (inset of Fig. 2c). For PBDTTT-CF, it is not readily possible to separate hole and electron mobilities, because no distinct change of $\sum\mu$ was observed over the range of PCBM content studied. This implies that the local hole and electron mobilities are always balanced at *ca.* 0.1 $cm^2\ V^{-1}\ s^{-1}$, which may underscore the success of PBDTTT-CF in OPVs. For PTzBT-BOHD, $\sum\mu$ was almost constant at 0.25 $cm^2\ V^{-1}\ s^{-1}$ from 23 to 95 wt% PCBM, which includes the device-optimal blend ratio (1 : 2, 67 wt%), and then decreased to 0.1 $cm^2\ V^{-1}\ s^{-1}$ at 100 wt% PCBM. Accordingly, the approximate local hole mobility of 0.15 (=0.25–0.1) $cm^2\ V^{-1}\ s^{-1}$ was deduced for the PTzBT-BOHD:PCBM blends. The crystalline nature of PTzBT-BOHD is highlighted from the view that solvent additive is unnecessary to achieve optimized morphology and the polymer has a prominent face-on orientation that is beneficial for hole transport in the vertical direction.[42] The tendency of PTzBT-BOHD to self-assemble would facilitate the formation of superior BHJ networks similar to P3HT.

Correlating $\sum\mu$ with device performance

The correlation between $\sum\mu$ and device performance (PCE/V_{oc}) was examined. This parameter is equivalent to the product of the short circuit current density (J_{sc}) and the fill factor (FF), and as such reflects the extent of charge carrier generation, mobility, and extraction. Fig. 3a shows PCE/V_{oc} as a function of $\sum\mu$ for seven pure polymers (also summarized in Table S1, ESI†). $\sum\mu$ is scattered over three orders of magnitude (10^{-2}–10^{0} $cm^2\ V^{-1}\ s^{-1}$). In particular, PBTTT-C_{14} has an exceptionally high TRMC mobility in the absence of PCBM. A similarly poor correlation has been reported between PCE and long-range mobilities estimated using FETs and the space-charge limited current (SCLC).[43]

In contrast, the plots of $\sum\mu$ for polymer:PCBM blends demonstrate an improved correlation, where the local mobility of the blend is more important for the OPV output than those of the pure polymers (Fig. 3b and Table S1, ESI†). Moreover, it was noted that the correlation includes two trends: that for crystalline polymers (P3HT, PBTTT-C_{14}, PQT-12, PTzBT-BOHD, PTzBT-14HD, and PTzBT-14OD) and that for semi-crystalline polymers (PCPDTBT, PCDTBT, PBDTTT-CF, and PSBTBT). This trend is not simply linked to whether the polymer is a push-pull type, because the crystalline PTzBT polymer is composed of electron-donating (bithiophene) and electron-withdrawing (thiazolothiazole) units.

To quantitatively examine these categories, X-ray diffraction (XRD) measurements of the blend films were performed (XRD spectra and values are provided in Fig. S6 and Table S2, ESI†). The mean size of polymer crystallite (correlation length) in the inter-lamellar direction, $L_{(100)}$ were evaluated using Scherrer

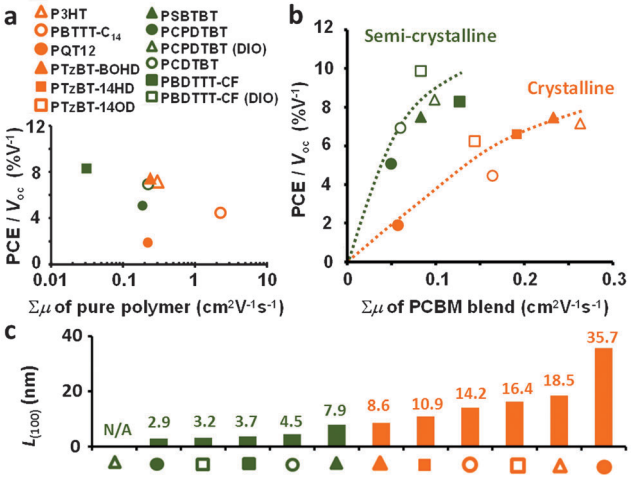

Fig. 3 Correlation between $\sum\mu$ and OPV performance for polymer:PCBM blends. (a) PCE/V_{oc} *vs.* $\sum\mu$ for the pure polymers. (b) Correlation of PCE/V_{oc} with $\sum\mu$ for the polymer:PCBM blends. The polymer : PCBM blend ratio was similar for both OPV and $\sum\mu$ evaluations. (c) Correlation length $L_{(100)}$ evaluated from the inter-lamellar XRD peaks of device-optimal polymer:PCBM blends in the out-of-plane direction. The data values and spectra are given in Table S2 and Fig. S6 (ESI†), respectively.

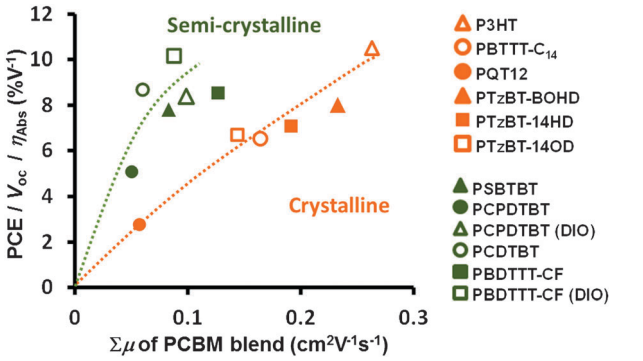

Fig. 4 Correlation of PCE/V_{oc}/η_{Abs} with $\sum\mu$ for the polymer:PCBM blends. See Table S3 and Fig. S8 (ESI†) for the calculation of η_{Abs}.

equation (Fig. 3c).[44] The crystalline polymers have larger $L_{(100)}$ values of 9–36 nm than those of semi-crystalline (or amorphous) polymers (<8 nm). In addition, the peak intensity, which corresponds to an inter-lamellar distance of 1.4–2.8 nm, can be also used to approximately distinguish the crystalline and semi-crystalline polymers (Fig. S7, ESI†). Actually, the boundary in both $L_{(100)}$ and peak intensity is likely unclear, which might be due to the effect of disordered phase inert to XRD measurement and/or limitation only in the out-of-plane direction. Interestingly, Ohkita *et al.* has reported the pronounced effect of crystallite size on the charge dissociation efficiency, where the total dissociation efficiency is increased with the correlation length in the π-stack direction, $L_{(010)}$, from 0.7 for disordered PCPDTBT, 0.75 for semi-crystalline PSBTBT, and 0.93 for crystalline P3HT.[45] They also have pointed out the important role of hole and/or electron delocalisation to liberate Coulomb-bound excitons. We thus speculate that the observed positive correlation between the TRMC local charge carrier mobility and PCE/V_{oc} can be linked to the correlation length of crystallite and resultant charge delocalisation.

Since the bandgaps of push-pull type semi-crystalline polymers are lower than those of crystalline polymers, we considered compensation of the absorption efficiency (η_{abs}) according to the bandgap energy of each polymer (details are provided in Fig. S8 and Table S3, ESI†). Fig. 4 shows the plot of PCE/V_{oc}/η_{abs} against $\sum\mu$ of the polymer:PCBM blend films. The crystalline polymers converged to give a straight line, while the semi-crystalline polymers were mostly unchanged. Compensation of the charge transport and collection efficiency (η_{CC}) were also examined using the Hecht expression,[46] charge carrier lifetime obtained by TRMC, and long-range mobilities of the SCLC or FET. However, the trend became considerably distorted (Fig. S9 and Table S4, ESI†), apparently due to the large deviation of these values that were independently determined by different groups using different methods.

Semi-crystalline and amorphous polymers generally have lower mobilities than crystalline polymers at the local and long-range scales. However, the OPV performance of semi-crystalline polymers is comparable or even better than that for crystalline polymers. The present study suggests that an increase in polymer crystallinity does not effectively improve η_{CS} and PCE. High crystallinity can improve both the long-range mobility associated with η_{CC} and the local mobility associated with η_{CS}. Conversely, the morphology of the donor/acceptor interface and exciton diffusion efficiency are assumed to be changed, which may weaken the advantage of high local mobility. In this case, hot CT excitons with large radii,[17] molecular orbital coupling between polymers and PCBM,[47] the presence of an amorphous donor/acceptor mixed phase with a downhill energy gradient,[20] and a gradual relaxation into the disordered density of state (DOS)[21] effectively assist CS in addition to the high local mobility.

In principle, light-induced TRMC and terahertz (THz) conductivity measurements probe the sum of hole and electron mobilities, which is usually disadvantageous when compared with unipolar FET and SCLC measurements. However, in the CS process between two opposite charges, the sum of the hole and electron mobilities are mathematically treated as one mutual mobility, which is compatible with AC mobility measurements. Therefore, the contribution of mobile electrons is implicitly included in the present measurement. For PQT-12 and PBTTT-C_{14}, it was surmised that the mobility at the optimal polymer : PCBM blend ratio is mainly attributed to electrons, while both holes and electrons are involved in P3HT and PTzBT-BOHD. Isotropic diffusion of mobile electrons in PCBM crystallites can facilitate the CS process;[48,49] however, it is not the sole determinant, because the OPV output and TRMC mobilities are still affected by the counter polymer, and in particular its crystallinity.

Although a good correlation of local mobility with the OPV output was observed, there is the possibility of further correlation of the local mobility with other physical properties such as delocalisation of the CT state[17,18] and the resonant coupling of photogenerated singlet excitons to a high-energy manifold of

fullerene aggregates.[47] A large sized polymer crystallite requires a long distance for the polymer exciton to reach the donor/acceptor interface, impeding the exciton diffusion efficiency (η_{ED}). The degree of fluorescence quenching is direct evidence, for instance, the value of η_{ED} of amorphous regiorandom P3HT, PCPDTBT, and semi-crystalline PSBTBT are $\sim$1, while that of crystalline P3HT is $\sim$0.9.[45] As mentioned previously, the hierarchical phase and energy gradient in the polymer:fullerene mixed domain, amorphous, and crystallite domains are important for efficient charge separation.[41] In addition to the presence of high local mobility probed using terahertz,[20] electric field-induced second harmonic (EFISH),[50,51] and gigahertz electromagnetic waves,[52] control of the polymer/fullerene interface is presumed to be of particular importance with respect to the energetics[53–56] and morphology suitable for efficient charge separation.

Conclusion

The local charge carrier mobility ($\sum\mu$) of BHJ films was experimentally determined using TRMC and PC techniques. $\sum\mu$ was subject to alteration by the polymer backbone, side-chain, donor/acceptor blend ratio, and the intercalation of PCBM. It was demonstrated that PCE/V_{oc} is correlated with the value of $\sum\mu$ of the polymer:PCBM blends rather than those of the pure polymers. Furthermore, this correlation exhibits two trends for the crystalline (P3HT, PQT-12, PBTTT-C_{14}, PTzBT) and semi-crystalline polymers (PCDTBT, PCPDTBT, PBDTTT-CF, PSBTBT), which can be linked to the size of the polymer crystallite determined from the XRD measurements. The underlying correlation has wide implications for the importance of the role of local charge carrier mobility associated with charge delocalisation and the size of the crystallite in the CS process, and for the design of highly-efficient polymer:fullerene OPVs.

Experimental

Materials

Regioregular poly(3-hexylthiophene) (P3HT; >98% head-to-tail regioregularity), and PCBM (purity >99.5%) were purchased from Aldrich and Frontier Carbon Inc., respectively. Thiazolothiazole–bithiophene copolymers bearing 2-butyloctyl and 2-hexyldecyl chains (PTzBT-BOHD), *n*-tetradecanyl and 2-octyldodecyl chains (PTzBT-14OD), and *n*-octyldecanyl and 2-hexyldecyl chains (PTzBT-14HD) have been synthesized and characterized previously.[42] Poly[*N*-9″-hepta-decanyl-2,7-carbazole-*alt*-5,5-(4′,7′-di-2-thienyl-2′,1′,3′-benzothiadiazole)] (PCDTBT), poly[2,6-(4,4-bis-(2-ethylhexyl)-4*H*-cyclopenta[2,1-*b*;3,4-*b*′]dithiophene)-*alt*-4,7(2,1,3benzothiadiazole)] (PCPDTBT), poly-[4,8-bis-substituted-benzo[1,2-*b*:4,5-*b*′]dithiophene-2,6-diyl-*alt*-4-substituted-thieno[3,4-*b*]thiophene-2,6-diyl] (PBDTTT-CF, analogue to PTB7), poly(3,3‴-didodecylquaterthiophene) (PQT-12), and poly(2,5-bis(3-tetradecylthiophene-2-yl)thieno[3,2-*b*]-thiophene) (PBTTT-C_{14}), and poly[(4,4′-bis(2-ethylhexyl)dithieno-[3,2-*b*:2′,3′-*d*]silole)-2,6-diyl-*alt*-(2,1,3-benzothiadiazole)-4,7-diyl] (PSBTBT) were purchased from One-Material Inc. Solvents were purchased from Kishida Kagaku Corp. and used as received without further purification. XRD measurements were conducted using a Rigaku MiniFlex600 with Cu Kα radiation (1.5418 Å).

Time-resolved microwave conductivity (TRMC) and transient photocurrent (PC) measurement

A BHJ film prepared by drop-casting (200–300 nm) on a quartz substrate was set in a resonant cavity and probed by continuous microwaves at *ca.* 9.1 GHz. The third harmonic generation (THG; 355 nm) of a Nd:YAG laser (Continuum Inc., Surelite II, 5–8 ns pulse duration, 10 Hz) was used as an excitation source (incident photon density, $I_0 = 4.6 \times 10^{15}$ photons cm^{-2} pulse^{-1}, 5 mm in diameter).[24] The photoconductivity transient $\Delta\sigma$ was converted to the product of the quantum efficiency (ϕ) and the sum of the charge carrier mobilities, $\sum\mu$ (= $\mu_+ + \mu_-$) by $\phi\sum\mu = \Delta\sigma(eI_0F_{light})^{-1}$, where e and F_{Light} are the unit charge of a single electron and a correction (or filling) factor, respectively. Details are reported in the literature.[22] An interdigitated comb-type gold electrode with 5 μm gaps, 50 nm height, and 2 mm width was fabricated on a glass substrate by a lithographic process in the laboratory and used for the PC experiments. After casting the sample, an electrode under direct-current electric bias was exposed to the THG of a Nd:YAG laser (Spectra Physics Inc. GCR-100, 5–8 ns pulse duration) from the back side with the same I_0. Transient PC decay was recorded with a resistance-terminated oscilloscope. ϕ was evaluated by comparing the PC maximum with that of a reference sample, poly(9,9′-dioctyl-fluorene), PDOF, according to a reported procedure.[31] Using a measured value of $\phi\sum\mu_{max}$ and the reported TRMC hole mobility of PDOF[57] ($\phi\sum\mu_{ref}$ and $\sum\mu_{ref}$, respectively), ϕ of a polymer:fullerene blend film (ϕ_{blend}) was calculated *via* $\phi_{blend} = \phi_{ref}(PC_{blend}/PC_{ref})$, whereas ϕ_{ref} is the reference value of PDOF ($\phi_{ref} = \phi\sum\mu_{ref}/\sum\mu_{ref}$) and PC_{ref} (PC_{blend}) is the transient PC maximum of the reference (blend). Our PC technique used the peak value of the PC transient (not from its integration over time), and was validated from the identical ϕ value with that estimated by another technique (transient absorption spectroscopy).[31] All experiments were conducted at room temperature.

Acknowledgements

This work was supported by the Precursory Research for Embryonic Science and Technology (PRESTO) program of the Japan Science and Technology Agency (JST), Tenure Track Program at the Frontier Research Base for Global Young Researchers of JST and Osaka University, and a Kakenhi Grant-in-Aid from the Ministry of Education (No. 25288084), Culture, Sports, Science and Technology (MEXT) of Japan.

References

1 L. Dou, J. You, Z. Hong, Z. Xu, G. Li, R. A. Street and Y. Yang, *Adv. Mater.*, 2013, **25**, 6642–6671.
2 J. E. Coughlin, Z. B. Henson, G. C. Welch and G. C. Bazan, *Acc. Chem. Res.*, 2014, **47**, 257–270.

3 N. Li, D. Baran, G. D. Spyropoulos, H. Zhang, S. Berny, M. Turbiez, T. Ameri, F. C. Krebs and C. J. Brabec, *Adv. Energy Mater.*, 2014, **4**, 1400084.
4 J. M. Szarko, B. S. Rolczynski, S. J. Lou, T. Xu, J. Strzalka, T. J. Marks, L. Yu and L. X. Chen, *Adv. Funct. Mater.*, 2014, **24**, 10–26.
5 L. Dou, J. You, J. Yang, C. C. Chen, Y. He, S. Murase, T. Moriarty, K. Emery, G. Li and Y. Yang, *Nat. Photonics*, 2012, **6**, 180–185.
6 T. Ameri, N. Li and C. J. Brabec, *Energy Environ. Sci.*, 2013, **6**, 2390–2413.
7 P. Müller-Buschbaum, *Adv. Mater.*, 2014, **26**, 7692–7709.
8 S. Mukhopadhyay, A. K. Das and K. S. Narayan, *J. Phys. Chem. Lett.*, 2013, **4**, 161–169.
9 S. D. Dimitrov and J. R. Durrant, *Chem. Mater.*, 2014, **26**, 616–630.
10 A. Tada, Y. Geng, Q. Wei, K. Hashimoto and K. Tajima, *Nat. Mater.*, 2011, **10**, 450–455.
11 P. K. Nayak, K. L. Narasimhan and D. Cahen, *J. Phys. Chem. Lett.*, 2013, **4**, 1707–1717.
12 C. Groves, *Energy Environ. Sci.*, 2013, **6**, 3202–3217.
13 D. Beljonne, J. Cornil, L. Muccioli, C. Zannoni, J.-L. Brédas and F. Castet, *Chem. Mater.*, 2011, **23**, 591–609.
14 T. M. Clarke and J. R. Durrant, *Chem. Rev.*, 2010, **110**, 6736–6767.
15 C. L. Braun, *J. Chem. Phys.*, 1984, **80**, 4157–4161.
16 S. H. Park, A. Roy, S. Beaupré, S. Cho, N. Coates, J. S. Moon, D. Moses, M. Leclerc, K. Lee and A. J. Heeger, *Nat. Photonics*, 2009, **3**, 297–303.
17 A. A. Bakulin, A. Rao, V. G. Pavelyev, P. H. M. van Loosdrecht, M. S. Pshenichnikov, D. Niedzialek, J. Cornil, D. Beljonne and R. H. Friend, *Science*, 2012, **335**, 1340–1344.
18 S. Yamamoto, H. Ohkita, H. Benten and S. Ito, *J. Phys. Chem. C*, 2012, **116**, 14804–14810.
19 B. A. Gregg, *J. Phys. Chem. Lett.*, 2011, **2**, 3013–3015.
20 T. M. Burke and M. D. McGehee, *Adv. Mater.*, 2014, **26**, 1923–1928.
21 H. van Eersel, R. A. J. Janssen and M. Kemerink, *Adv. Funct. Mater.*, 2012, **22**, 2700–2708.
22 A. Saeki, Y. Koizumi, T. Aida and S. Seki, *Acc. Chem. Res.*, 2012, **45**, 1193–1202.
23 T. J. Savenije, A. J. Ferguson, N. Kopidakis and G. Rumbles, *J. Phys. Chem. C*, 2013, **117**, 24085–24103.
24 A. Saeki, M. Tsuji and S. Seki, *Adv. Energy Mater.*, 2011, **1**, 661–669.
25 M. Tsuji, A. Saeki, Y. Koizumi, N. Matsuyama, C. Vijayakumar and S. Seki, *Adv. Funct. Mater.*, 2014, **24**, 28–36.
26 A. Saeki, S. Yoshikawa, M. Tsuji, Y. Koizumi, M. Ide, C. Vijayakumar and S. Seki, *J. Am. Chem. Soc.*, 2012, **134**, 19035–19042.
27 D. Veldman, Ö. Ípek, S. C. J. Meskers, J. Sweelssen, M. M. Koetse, S. C. Veenstra, J. M. Kroon, S. S. van Bavel, J. Loos and R. A. J. Janssen, *J. Am. Chem. Soc.*, 2008, **130**, 7721–7735.
28 C. Deibel, T. Strobel and V. Dyakonov, *Phys. Rev. Lett.*, 2009, **103**, 036402.
29 W. L. Rance, A. J. Ferguson, T. McCarthy-Ward, M. Heeney, D. S. Ginley, D. C. Olson, G. Rumbles and N. Kopidakis, *ACS Nano*, 2011, **5**, 5635–5646.
30 A. A. Bakulin, S. D. Dimitrov, A. Rao, P. C. Y. Chow, C. B. Nielsen, B. C. Schroeder, I. McCulloch, H. J. Bakker, J. R. Durrant and R. H. Friend, *J. Phys. Chem. Lett.*, 2013, **4**, 209–215.
31 Y. Yasutani, A. Saeki, T. Fukumatsu, Y. Koizumi and S. Seki, *Chem. Lett.*, 2013, **42**, 19–21.
32 N. C. Cates, R. Gysel, Z. Beiley, C. E. Miller, M. F. Toney, M. Heeney, I. McCulloch and M. D. McGehee, *Appl. Phys. Lett.*, 2008, **92**, 113309.
33 B. H. Hamadani, D. J. Gundlach, I. McCulloch and M. Heeney, *Appl. Phys. Lett.*, 2007, **91**, 243512.
34 N. C. Miller, E. Cho, M. J. N. Junk, R. Gysel, C. Risko, D. Kim, S. Sweetnam, C. E. Miller, L. J. Richter, R. J. Kline, M. Heeney, I. McCulloch, A. Amassian, D. Acevedo-Feliz, C. Knox, M. R. Hansen, D. Dudenko, B. F. Chmelka, M. F. Toney, J.-L. Brédas and M. D. McGehee, *Adv. Mater.*, 2012, **24**, 6071–6079.
35 M. P. de Haas, J. M. Warman, T. D. Anthopoulos and D. M. de Leeuw, *Adv. Funct. Mater.*, 2006, **16**, 2274–2280.
36 A. J. Moulé, S. Allard, N. M. Kronenberg, A. Tsami, U. Scherf and K. Meerholz, *J. Phys. Chem. C*, 2008, **112**, 12583–12589.
37 C. Bruner, N. C. Miller, M. D. McGehee and R. H. Dauskardt, *Adv. Funct. Mater.*, 2013, **23**, 2863–2871.
38 B. S. Ong, Y. Wu, P. Liu and S. Gardner, *Adv. Mater.*, 2005, **17**, 1141–1144.
39 G. Wang, J. Swensen, D. Moses and A. J. Heeger, *J. Appl. Phys.*, 2003, **93**, 6137–6141.
40 N. D. Treat, M. A. Brady, G. Smith, M. F. Toney, E. J. Kramer, C. J. Hawker and M. L. Chabinyc, *Adv. Energy Mater.*, 2011, **1**, 82–89.
41 J. Jo, S.-S. Kim, S.-I. Na, B.-K. Yu and D.-Y. Kim, *Adv. Funct. Mater.*, 2009, **19**, 866–874.
42 I. Osaka, M. Saito, T. Koganezawa and K. Takimiya, *Adv. Mater.*, 2014, **26**, 331–338.
43 R. Lecover, N. Williams, N. Markovic, D. H. Reich, D. Q. Naiman and H. E. Katz, *ACS Nano*, 2012, **6**, 2865–2870.
44 T. Erb, U. Zhokhavets, G. Gobsch, S. Raleva, B. Stühn, P. Schilinsky, C. Waldauf and C. J. Brabec, *Adv. Funct. Mater.*, 2005, **15**, 1193–1196.
45 Y. Tamai, K. Tsuda, H. Ohkita, H. Benten and S. Ito, *Phys. Chem. Chem. Phys.*, 2014, **16**, 20338–20346.
46 R. A. Street, M. Schoendorf, A. Roy and J. H. Lee, *Phys. Rev. B: Condens. Matter Mater. Phys.*, 2010, **81**, 205307.
47 B. M. Savoie, A. Rao, A. A. Bakulin, S. Gélinas, B. Movaghar, R. H. Friend, T. J. Marks and M. A. Ratner, *J. Am. Chem. Soc.*, 2014, **136**, 2876–2884.
48 S. Albrecht, K. Vandewal, J. R. Tumbleston, R. S. U. Fischer, J. D. Douglas, J. M. J. Fréchet, S. Ludwigs, H. Ade, A. Salleo and D. Neher, *Adv. Mater.*, 2014, **26**, 2533–2539.
49 F. C. Jamieson, E. B. Domingo, T. McCarthy-Ward, M. Heeney, N. Stingelin and J. R. Durrant, *Chem. Sci.*, 2012, **3**, 485–492.
50 D. A. Vithanage, A. DeviŽis, V. Abramavičius, Y. Infahsaeng, D. Abramavičius, R. C. I. MacKenzie, P. E. Keivanidis, A. Yartsev, D. Hertel, J. Nelson, V. Sundström and V. Gulbinas, *Nat. Commun.*, 2013, **4**, 2334.

51 V. Abramavičius, D. A. Vithanage, A. Devižis, Y. Infahsaeng, A. Bruno, S. Foster, P. E. Keivanidis, D. Abramavičius, J. Nelson, A. Yartsev, V. Sundström and V. Gulbinas, *Phys. Chem. Chem. Phys.*, 2014, **16**, 2686–2692.

52 J. C. Aguirre, C. Arntsen, S. Hernandez, R. Huber, A. M. Nardes, M. Halim, D. Kilbride, Y. Rubin, S. H. Tolbert, N. Kopidakis, B. J. Schwartz and D. Neuhauser, *Adv. Funct. Mater.*, 2014, **24**, 784–792.

53 G. D'Avino, S. Mothy, L. Muccioli, C. Zannoni, L. Wang, J. Cornil, D. Beljonne and F. Castet, *J. Phys. Chem. C*, 2013, **117**, 12981–12990.

54 S. V. Kesava, Z. Fei, A. D. Rimshaw, C. Wang, A. Hexemer, J. B. Asbury, M. Heeney and E. D. Gomez, *Adv. Energy Mater.*, 2014, **4**, 1400116.

55 Y. Kobori, R. Noji and S. Tsuganezawa, *J. Phys. Chem. C*, 2013, **117**, 1589–1599.

56 A. V. Nenashev, S. D. Baranovskii, M. Wiemer, F. Jansson, R. Österbacka, A. V. Dvurechenskii and F. Gebhard, *Phys. Rev. B: Condens. Matter Mater. Phys.*, 2011, **84**, 035210.

57 F. C. Grozema, L. D. A. Siebbeles, J. M. Warman, S. Seki, S. Tagawa and U. Scherf, *Adv. Mater.*, 2002, **14**, 228–231.

